



Contents lists available at ScienceDirect

Applied Catalysis B: Environmental

journal homepage: www.elsevier.com/locate/apcatb



Synergistic effect of bimetallic Au-Pd supported on ceria-zirconia mixed oxide catalysts for selective oxidation of glycerol

Carol M. Olmos^a, Lidia E. Chinchilla^a, Elodie G. Rodrigues^b, Juan J. Delgado^a, Ana B. Hungría^a, Ginesa Blanco^a, Manuel F.R. Pereira^b, José J.M. Órfão^b, Jose J. Calvino^a, Xiaowei Chen^{a,*}

^a Departamento de Ciencia de los Materiales, Ingeniería Metalúrgica y Química Inorgánica, Facultad de Ciencias, Universidad de Cádiz, Campus Río San Pedro, Puerto Real (Cádiz), E-11510, Spain

^b Laboratory of Separation and Reaction Engineering—Laboratory of Catalysis and Materials (LSRE-LCM), Faculty of Engineering, University of Porto, Rua Dr. Roberto Frias, 4200-465 Porto, Portugal

ARTICLE INFO

Article history:

Received 30 November 2015

Received in revised form 26 February 2016

Accepted 23 March 2016

Available online xxxx

Keywords:

Glycerol oxidation
Gold
Palladium
Bimetallic catalyst
Ceria-zirconia

ABSTRACT

A series of bimetallic Au-Pd catalysts supported on $\text{Ce}_{0.62}\text{Zr}_{0.38}\text{O}_2$ mixed oxide has been synthesized using a simultaneous deposition-precipitation method. Different Au:Pd ratios were obtained maintaining Au loadings constant and varying Pd content. Elemental analysis, X-ray diffraction, N_2 physisorption, X-ray photoelectron spectroscopy, scanning transmission electron microscopy-high angle annular dark field (STEM-HAADF) and X-ray energy dispersive spectroscopy (XEDS) techniques have been employed to characterize these catalysts. The catalytic activities for selective oxidation of glycerol over these bimetallic catalysts have been evaluated, a synergistic effect being observed. Thus, the bimetallic Au-Pd catalyst with the lowest Pd content was the one exhibiting the highest catalytic activity among all the prepared catalysts. Oxidation at 700 °C of the bimetallic 2.2AuPd/ $\text{Ce}_{0.62}\text{Zr}_{0.38}\text{O}_2$ catalyst led to an increase of the catalytic activity for the selective oxidation of glycerol, which seemed to be due to the formation of a larger fraction of bimetallic Au-Pd alloy-type nanoparticles after oxidation at higher temperatures.

© 2016 Elsevier B.V. All rights reserved.

1. Introduction

In recent years, selective oxidation of glycerol to high-value chemicals with molecular oxygen has attracted a lot of attention because glycerol is the main by-product from the production of biodiesel [1–3], which is considered as a sustainable clean fuel to substitute fossil energy. Glycerol oxidation may produce glyceric acid, glycolic acid, dihydroxyacetone, tartronic acid, glyceraldehyde, lactic acid, oxalic acid, etc. [1–3]. However, the similarity of reactive hydroxyl groups in the glycerol molecule hinders the development of catalysts with high conversion and high selectivity towards products with actual industrial interest [2]. Therefore, selectivity control of glycerol oxidation is highly desirable for its further industrial application.

Supported noble metals (Au, Pt, Pd, Rh and Ir) have been extensively investigated as catalysts for selective oxidation of glycerol [4–16]. Monometallic Pt and Pd supported on activated carbon

catalysts exhibit good selectivity of 55% and 70% to glyceric acid, respectively [5]. The main drawback of Pt and Pd catalysts is a deactivation problem with reaction time due to oxygen poisoning [3]. Au catalysts show better resistance to oxygen poisoning, which permits using high oxygen partial pressures [17]. Furthermore, the selectivity to glyceric acid reaches 100% over Au supported on activated carbon and graphite catalysts with total glycerol conversion of 56% [6]. Bimetallic Au-Pd or Au-Pt catalysts combine the advantages of both metals and demonstrate synergistic effect for the selective oxidation of glycerol [12,13,15,16,18–20].

The catalytic activity for glycerol oxidation seems to be significantly influenced by the nature of metal, metal particle size and support of the bimetallic Au-Pd catalysts. On the other hand, these parameters also strongly depend on the preparation method. A single-phase bimetallic Au-Pd on activated carbon catalyst has been synthesized with a two-step sol immobilization method by Prati's group [18], namely, a Au sol was firstly immobilized on activated carbon (AC) using NaBH_4 as reducing agent and then a Pd sol was generated in the presence of Au/AC using H_2 as reducing agent. Synergistic effects between Au and Pd have been observed in a wide range of Au:Pd ratios (from 1:4 to 9.5:0.5), which were attributed

* Corresponding author.

E-mail address: xiaowei.chen@uca.es (X. Chen).

Table 1

Codings and chemical-physical properties of the monometallic and bimetallic catalysts.

Catalyst	Au loading (wt%) ^a	Pd loading (wt%) ^a	Nominal Au:Pd molar ratio	Actual Au:Pd molar ratio ^a	S_{BET} ($\text{m}^2 \text{g}^{-1}$)	Average particle size ^b (nm)	Metal dispersion ^b (%)	Au:Pd molar ratio ^c	TOF _{TOTAL} ^d (h^{-1})	TOF _{TEM} ^e (h^{-1})
Au/CZ	2.5	–	–	–	64	1.7 ± 0.1	39	–	128	328
0.8AuPdCZ	2.4	1.6	1:1	0.8:1(44 mol% Au)	65	2.1 ± 0.1	36	2.5:1	61	169
2.2AuPdCZ	2.1	0.5	3:1	2.2:1(68 mol% Au)	64	2.6 ± 0.1	37	8.2:1	126	314
6.4AuPdCZ	2.0	0.2	10:1	6.4:1(86 mol% Au)	64	2.3 ± 0.1	34	33.8:1	175	515
Pd/CZ	–	1.2	–	–	66	1.9 ± 0.1	45	–	102	227

^a The Au and Pd loadings were determined by ICP analysis.^b Average particle size and metal dispersion were determined by STEM technique.^c Au:Pd molar ratio was obtained by STEM-XEDS.^d TOF_{TOTAL} values were calculated based on total amount of metals of the catalysts when the reaction time is 3 h.^e TOF_{TEM} values were calculated based on the metal dispersion obtained by STEM-HAADF when the reaction time is 3 h.

to the presence of alloy phases [19]. With an increase of Au content, the activity increases distinctly and reaches a maximum for Au:Pd = 9:1 [19]. The same group also prepared bimetallic Au-Pd sol reduced by N₂H₄-2HCl and NaBH₄ using different time and then immobilized them on AC [21]. The bimetallic Au-Pd catalyst prepared by a one-step immobilization process and further reduced by NaBH₄ for 6 h produced showed higher TOF values and smaller metal particle size than the bimetallic catalysts reduced by NaBH₄ for 19 h and reduced by N₂H₄-2HCl [21]. Bimetallic Au-Pd catalysts supported on carbon and titania were also prepared by Hutchings' group, using simultaneous impregnation method [22]. In comparison to impregnation, sol immobilization method leads to catalysts with higher activity [22].

Until now, the most commonly studied supports for glycerol oxidation are carbon based materials, such as activated carbon [4,5,8,12,13,18,19,21], graphite [6,13], or carbon nanotubes [9,10]. Only a few studies have focused on oxide-based supports, for example, titania [22–24], ceria [24–26], or Mg-Al mixed oxide [27]. Au/CeO₂ catalyst prepared using deposition-precipitation with urea followed by reduction with glycerol shows unique selectivity (more than 70%) to lactic acid [25]. It is commonly agreed that the incorporation of Zr in ceria improve its redox property due to the ability of ceria to switch between Ce⁴⁺ and Ce³⁺ oxidation states [28]. Recently, a synergistic effect was reported over bimetallic Au-Ru supported on ceria-zirconia catalysts for glycerol oxidation [29].

In our group, monometallic Au and bimetallic Au-Pd supported on ceria-zirconia mixed oxide catalysts with small metal particle size (less than 5 nm) have been extensively studied [30–35]. In this work, bimetallic Au-Pd supported on ceria-zirconia catalysts with different Au:Pd molar ratios in the range from 0.8 to 6.4 have been synthesized by simultaneous deposition-precipitation method. The catalytic performance for glycerol oxidation of these Au-Pd catalysts has been evaluated. To the best of our knowledge, bimetallic Au-Pd supported on ceria-zirconia catalysts have not been investigated yet for selective oxidation of glycerol.

2. Experimental

2.1. Catalyst preparation

The precursors, HAuCl₄·3H₂O (99.99%) and PdCl₂ (99.99%), were supplied by Alfa-Aesar and Sigma-Aldrich, respectively. The Ce_{0.62}Zr_{0.38}O₂ support was provided by Grace Davison. The preparation method of the reference monometallic Au and Pd supported on ceria-zirconia has been described in our previous work [35].

The reference monometallic 2.5 wt.% Au/Ce_{0.62}Zr_{0.38}O₂ catalyst was prepared by deposition-precipitation method with Na₂CO₃ as precipitating agent (This catalyst is coded as Au/CZ) [35]. The second reference sample, a monometallic 1.2 wt.%Pd/Ce_{0.62}Zr_{0.38}O₂ catalyst was prepared using incipient wetness impregnation method with an aqueous solution of Pd(NO₃)₂·4NH₃. The impregnated sample was dried at 100 °C overnight, calcined at 350 °C for 4 h in a muffle oven and finally reduced at 350 °C with 5% H₂/Ar for 1 h. This catalyst is coded as Pd/CZ [35].

The bimetallic Au-Pd catalysts with different Au:Pd ratios were prepared using simultaneous deposition-precipitation method. PdCl₂ was dissolved in a 1 M HCl solution and then mixed with the aqueous solution of HAuCl₄. The theoretical Au:Pd molar ratios were 1, 3 and 10 keeping always HAuCl₄ concentration constant (3.2 mM). Using a liquid pump, the mixture of HAuCl₄ and PdCl₂ solutions was added to a flask containing 15 g of the Ce_{0.62}Zr_{0.38}O₂ support suspended in 800 mL deionized water. At the same time, an automatic titrator TIM 856 was used to adjust and maintain the pH value at 8 with an aqueous Na₂CO₃ solution of 0.05 M. The samples were filtered and washed several times with deionized water at room temperature until no chloride ions could be detected with AgNO₃. The samples were subsequently dried at 100 °C overnight. The dried catalysts were oxidized in a flow of 5% O₂/He for 1 h at 250 °C with a heating rate of 10 °C min⁻¹. After this oxidation step, the gas flow was switched to He at the same temperature for 1 h. Then the catalysts were cooled down to room temperature under the inert gas flow. The Au and Pd loadings and Au:Pd ratios of the catalysts are listed in Table 1. The Au-Pd/Ce_{0.62}Zr_{0.38}O₂ catalysts with actual Au:Pd molar ratios of 0.8, 2.2 and 6.4 are referred as to 0.8AuPdCZ, 2.2AuPdCZ and 6.4AuPdCZ, respectively. The as-synthesized bimetallic 2.2AuPdCZ catalyst was also oxidized in a flow of 5% O₂/He at 350, 450 and 700 °C for 1 h in order to investigate the effect of oxidation temperature. In the following, these catalysts are coded as 2.2AuPdCZO350, 2.2AuPdCZO450 and 2.2AuPdCZO700, respectively.

2.2. Catalyst characterization

Textural properties of the catalysts were determined by N₂ adsorption at -196 °C using Micromeritics ASAP2020. Inductively coupled plasma-atomic emission spectrometry (ICP-AES) was employed to determine the Au and Pd loadings of the catalysts. X-ray diffraction (XRD) analyses of the catalysts were carried out using a Bruker diffractometer Model D8 ADVANCE operated at 40 kV and 40 mA employing Cu K α radiation.

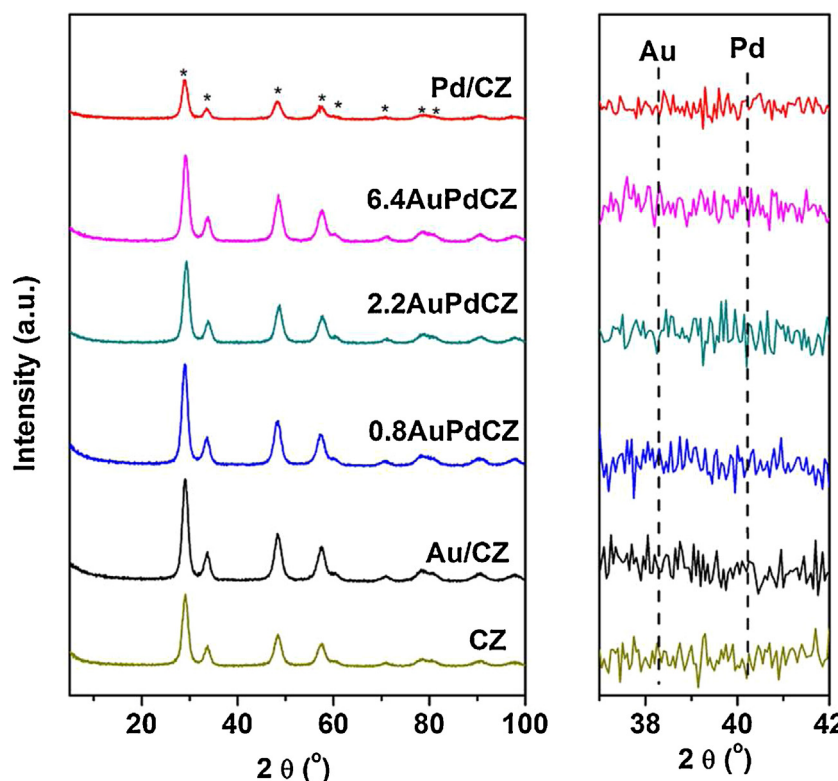


Fig. 1. XRD patterns of monometallic Au/CZ, Pd/CZ and bimetallic Au-Pd catalysts with different Au:Pd molar ratios. * Diffraction peaks of fluorite structure for Ce_{0.62}Zr_{0.38}O₂ mixed oxide.

X-ray photoelectron spectroscopy (XPS) analyses were performed on a Kratos Axis Ultra DLD instrument. Spectra were recorded using monochromatized Al K α radiation (1486.6 eV), with an X-ray power of 150 W. The spectrometer was operated in the Constant Analyser Energy mode, with a pass energy of 20 eV. Powder samples were pressed into pellets, which were stuck on a double-sided adhesive conducting polymer tape. Surface charging effects were compensated by making use of the Kratos coaxial neutralization system. The binding energy (BE) scale was calibrated with respect to the Zr 3d_{5/2} component of the mixed oxide support, and fixed at 182.64 eV as reported in [30]. XPS data analysis was performed with CasaXPS Software, version 2.3.17dev6.3a, developed by Neal Fairley (Casa Software Ltd, 2013).

Transmission electron microscopy experiments were performed on a JEOL2010 field emission gun instrument equipped with an Oxford INCA Energy 2000 XEDS spectrometer. STEM-HAADF images, whose intensity is roughly proportional to the square of the atomic number (Z^2), were recorded by using an electron probe of 0.5 nm of diameter at a diffraction camera length of 8 cm. Based on the STEM-HAADF images of the Au-containing catalysts, the diameters of more than 200 metal particles randomly selected were measured and the corresponding metal particle size distributions were determined. The average particle diameter (d) and the metal dispersion were calculated assuming a truncated cuboctahedron particle shape using a home-made software (GAUSS) [34]. Around 70 individual particles were analyzed in each bimetallic catalyst by STEM-XEDS. The Au:Pd molar ratio and Au content of each bimetallic catalyst was also calculated using the size and composition data of each metal particle analyzed by XEDS.

2.3. Catalytic activity test of glycerol oxidation

The standard oxidation experiments were carried out with oxygen under 3 bar at 60 °C.

A NaOH solution (NaOH:glycerol molar ratio = 2) and catalyst (700 mg) were added to a 0.3 M aqueous solution of glycerol ($V = 150$ mL) under stirring at 1000 rpm. After heating under nitrogen to the selected temperature, the reaction was initiated by switching from inert gas to oxygen.

The reaction was monitored by taking samples (0.5 mL) for analysis at regular time intervals for 5–6 h. The quantitative analysis of the reaction mixtures was carried out by high performance liquid chromatography. The chromatograph (Elite LaChrom HITACHI) was equipped with a refractive index and an ultraviolet (210 nm) detector. Reactant and products were separated on an ion exclusion column (Alltech OA 1000). Products were identified by comparison with standard samples. Glycerol (>99.5%) was purchased from Fluka. Glyceric acid and the by-products glycolic acid, tartaric acid and oxalic acid were obtained from Sigma-Aldrich. The conversion and selectivity calculation details can be found elsewhere [10,11,14].

3. Results and discussion

3.1. Effect of Au:Pd ratio

3.1.1. BET surface areas and ICP results

Table 1 lists the BET specific surface areas and ICP results of the bimetallic catalysts with different Au:Pd molar ratios maintaining Au loadings constant. The Au:Pd molar ratios do not affect the BET specific surface areas, which are very similar to the surface area of the starting Ce_{0.62}Zr_{0.38}O₂ support (67 m² g⁻¹). The actual Pd loadings correspond exactly to the nominal values, indicating that there is no Pd loss during the preparation process. However, the actual Au loadings of the catalysts are lower than the nominal values. In fact, ICP analyses show the presence of Au in the filtered solutions from washing process. Therefore, the actual Au:Pd molar ratios of Au-Pd/Ce_{0.62}Zr_{0.38}O₂ catalysts are finally 0.8, 2.2 and 6.4. These

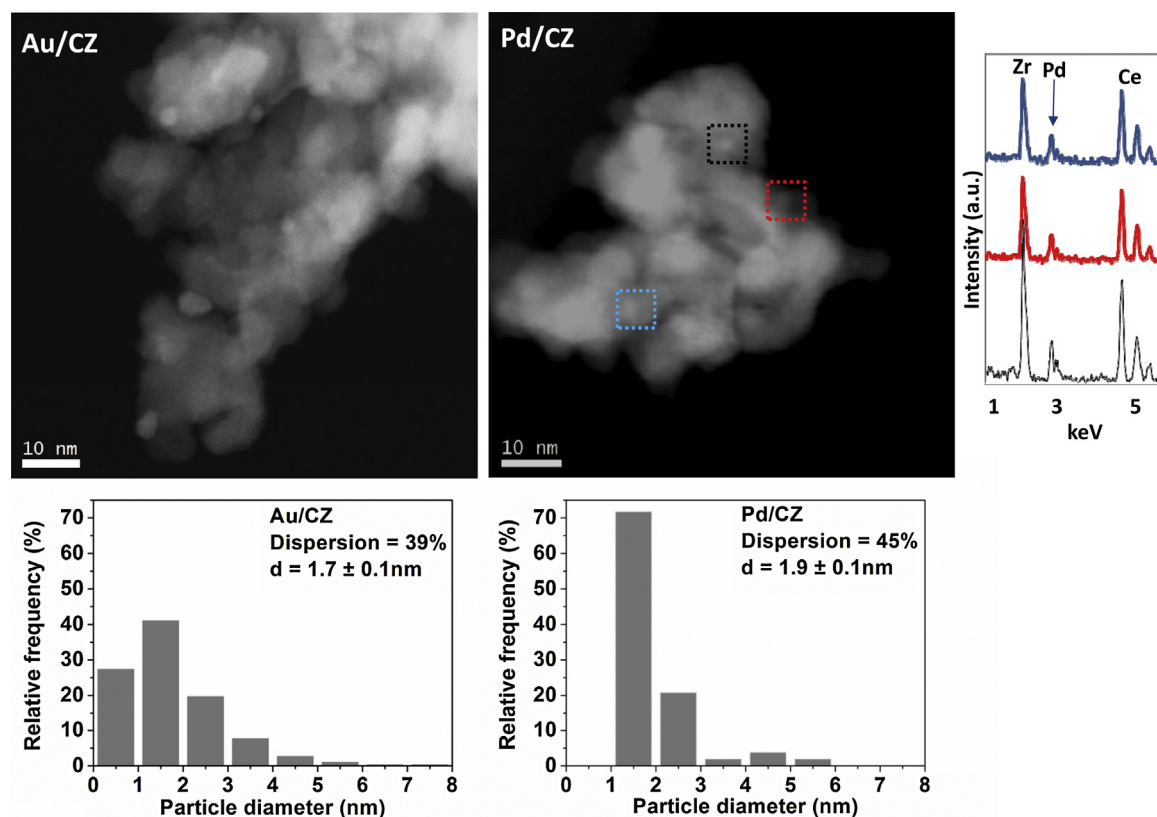


Fig. 2. STEM-HAADF images and particle size distribution of the monometallic Au/CZ and Pd/CZ catalysts. XEDS spectra of Pd/CZ catalyst in the selected analysis areas confirm the existence of small Pd particles.

values deviate, especially in the case of the highest, from the nominal ones: 1, 3 and 10.

3.1.2. X-ray diffraction results

Fig. 1 presents the XRD patterns of the support, monometallic and bimetallic catalysts with variable Au:Pd molar ratios. The diffraction peaks at 2θ values of 29.0, 33.5, 48.2, 57.5, 60.3, 70.8, 77.0 and 80.9, found on the support and on all the prepared catalysts, can be attributed to the crystallographic planes of a fluorite type ceria-zirconia mixed oxide [29,35]. There are no characteristics peaks of Pd, Au, PdO or Au-Pd alloy in the XRD patterns of these catalysts. The absence of any metal-related XRD peak suggests that the metal phases are well dispersed, in the form of very small nanoparticles.

3.1.3. STEM results

The metal dispersion and average particle size of the Au/CZ and Pd/CZ catalysts estimated from the particle size distributions are included in Table 1. Representative STEM-HAADF images of these two catalysts are shown in Fig. 2. The size of the metal particles in the Au/CZ catalyst ranges from 1 to 8 nm, with an average diameter of 1.7 nm and metal dispersion of 39% based on measurement of more than 200 Au nanoparticles.

It is important to indicate that the intensity in STEM-HAADF images depends roughly on Z^2 . Note at this respect that the values of atomic numbers are 46 (Pd), 58 (Ce), 40 (Zr) and 79 (Au), i.e. the HAADF signals generated by the support are slightly stronger ($Z_{\text{Ce}} \text{Ce}_{0.62} \text{Zr}_{0.38} \text{O}_2 \approx 51$) than those produced by the Pd atoms, but much weaker than those due to Au. Under these circumstances, for metallic particles of the same size and on crystals of support of the same thickness, the contrast between support and Pd will be smaller than between support and Au. In order to make sure the metal dispersion of Pd/CZ catalyst is properly calculated, 52

Pd particles with confirmation of XEDS analyses were counted and used to calculate the metal dispersion. The metal dispersion of this catalyst is 45% and the average particle size is 1.9 nm. This result is in good accordance with XRD results, which do not appear any Pd or PdO diffraction peak on this catalyst.

Fig. 3 shows representative STEM-HAADF images and particle size distributions of the bimetallic catalysts. The metal particle size of these catalysts falls in the 0.8–16 nm range and, in all cases, most of the particles are smaller than 5 nm. In fact, the differences in average metal particle size and metal dispersion values between the different bimetallic catalysts are below 5%. Thus, from a dimensional point of view, the metallic particle systems of the three bimetallic catalysts are very similar.

Three types of metal particles could be found: pure Au and Pd and bimetallic Au-Pd with varying compositions by STEM-XEDS technique. Fig. 3 illustrates the relative frequency of Au, Pd and bimetallic Au-Pd nanoparticles in the different bimetallic catalysts. The frequency of bimetallic Au-Pd particles observed in 0.8AuPdCZ, 2.2AuPdCZ and 6.4AuPdCZ were 92, 49 and 17%, respectively. Note that the fraction of bimetallic particles decreases with increasing Au:Pd ratio, i.e. higher Pd contents favor the formation of bimetallic particles. The Au content of the 0.8AuPdCZ catalyst is 44% according to ICP analysis. Nevertheless, as shown in the bottom part of Fig. 3, the Au content inside the bimetallic particles varies in a wide range, from 10 to 92%. These bimetallic particles range in particle diameter from 0.5 to 6 nm, although most of them are smaller than 4 nm. This is also the case of the monometallic Pd particles in this catalyst.

Meanwhile, the frequency of Au nanoparticles increases with increasing Au:Pd ratio. Thus, 43% of the metal particles are monometallic Au in 2.2AuPdCZ and 79% in 6.4AuPdCZ. Monometallic Au particles found in these two catalysts are from 1.5 to 12 nm in diameter, which are bigger than Pd particles in range of 0.5–4 nm. Note that all the bimetallic particles in the three catalysts range

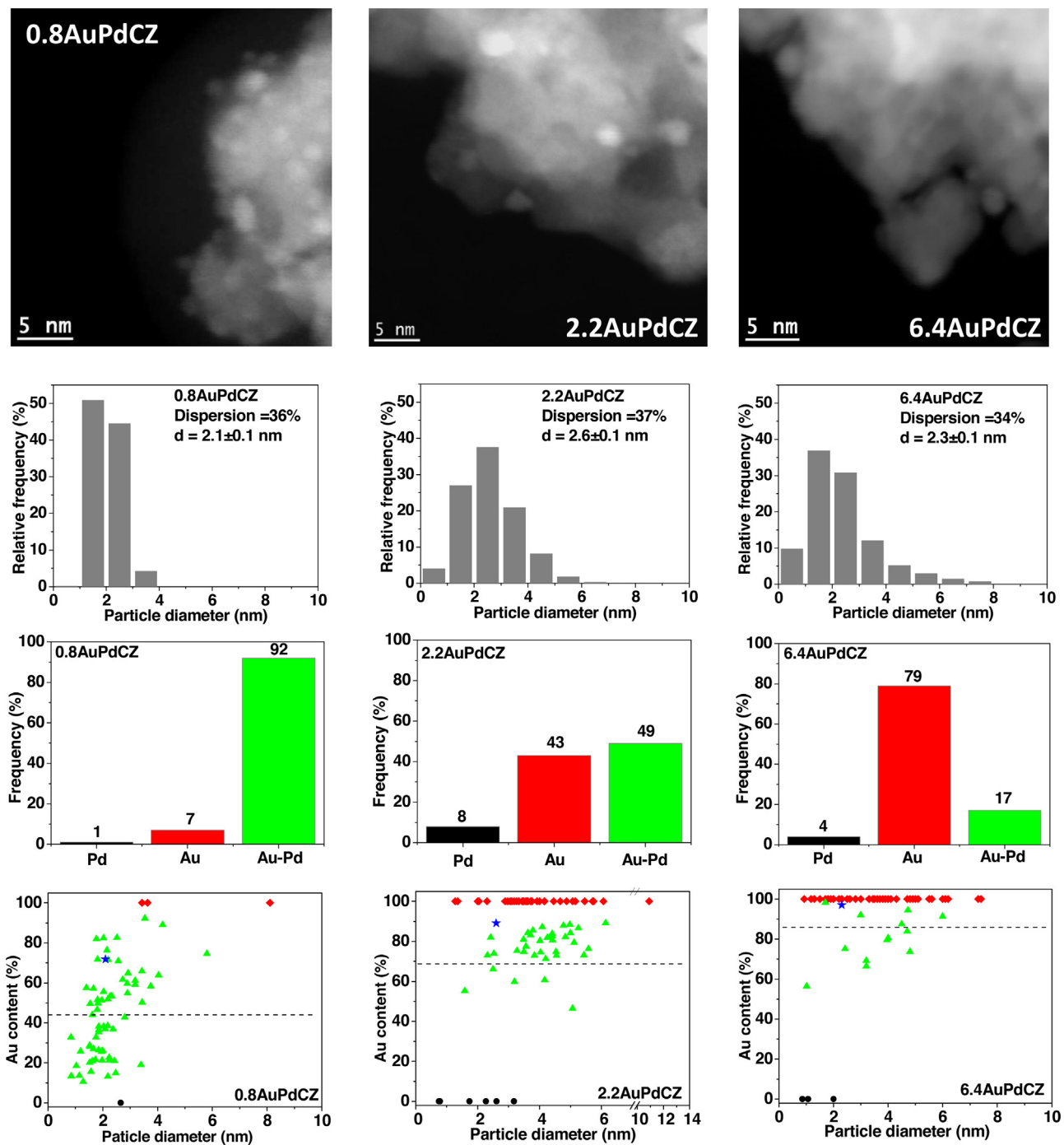


Fig. 3. STEM-HAADF images, particle size distribution, frequency of Au, Pd and Au-Pd metal particles, and relationship between particle size and Au content of 0.8AuPdCZ, 2.2AuPdCZ and 6.4AuPdCZ catalysts. The dash line is the Au content according to ICP analysis for each catalyst. Solid black circles correspond to monometallic Pd particles; solid red diamonds correspond to monometallic Au particles; solid green up-triangles correspond to bimetallic Au-Pd particles. Solid blue star corresponds to the average particle size and the average Au content calculated by XEDS data. (For interpretation of the references to colour in this figure legend, the reader is referred to the web version of this article.)

in size from 0.8 to 6.1 nm. The Au contents of the bimetallic particles in these two catalysts are 45–90% and 60–92%, respectively, i.e. in a narrower range around the corresponding values observed by ICP. This narrowing of the bimetallic particle composition with increasing Au:Pd ratio is clearly observed in the composition vs particle size diameter graphs included in Fig. 3. The Au:Pd molar ratio of each bimetallic catalyst was calculated based on the data of the particle composition and size as shown in Table 1. The Au:Pd molar ratios obtained by XEDS data are much higher than those estimated

by ICP results. As already commented before, the larger difficulties in the detection of Pd as compared to Au in the investigated catalysts might contribute to an underestimation of the fraction of Pd-rich nanoparticles (including monometallic Pd nanoparticles) over bimetallic Au-Pd catalysts. This is why Au:Pd molar ratios calculated by XEDS are lower than ICP results.

The STEM-XEDS results suggest that the used synthesis procedure, i.e. simultaneous deposition-precipitation and further oxidation at 250 °C, leads to compositionally heterogeneous par-

Table 2

Quantified XPS data of the monometallic and bimetallic catalysts with different Au:Pd ratios.

Catalyst	Ce ³⁺ in total amount of Ce (%)	Au 4f _{7/2} (eV)		Pd 3d _{5/2} (eV)		Molar ratios			
		Au ^o (%)	Au ^{δ+} (%)	Pd ^o (%)	Pd ^{δ+} (%)	Zr:Ce	Au:Zr	Pd:Zr	Au:Pd
Au/CZ	5	84.5 (77%)	85.4 (23%)	—	—	0.43	0.09	—	—
0.8AuPdCZ	33	84.1 (94%)	85.3 (6%)	336.1 (79%)	338.3 (21%)	0.44	0.17	0.40	0.44
2.2AuPdCZ	15	84.3 (89%)	85.2 (11%)	336.2 (55%)	338.3 (45%)	0.44	0.13	0.18	0.76
6.4AuPdCZ	4	84.4 (80%)	85.4 (20%)	336.2 (30%)	338.5 (70%)	0.42	0.11	0.08	1.40
Pd/CZ-O	8	—	—	336.6 (17%)	338.4 (83%)	0.43	—	0.14	—
Pd/CZ	14	—	—	336.2 (52%)	338.2 (48%)	0.42	—	0.10	—

ticle systems. According to Maeland and Flanagan's theory [36,37], the solubility of Au in Pd is of the order of 12 at.% whereas the maximum solubility of Pd in Au is higher, 31 at.%. The bimetallic 0.8AuPdCZ catalyst (44 mol% Au) is the only one with a nominal composition outside the solubility ranges. Moreover, the Au compositions observed in some of the bimetallic particles present in this catalyst (see bottom row in Fig. 3), are outside the composition ranges described in the literature [36,37]. For the other two catalysts, 2.2AuPdCZ (68 mol% Au) and 6.4AuPdCZ (86 mol% Au), the nominal compositions are within the maximum solubility limits and, on the other hand, most of the particles observed in these two catalysts have Au contents of 70–100 mol%, i.e. within this solubility limit. The 6.4AuPdCZ catalyst was particularly supposed to form homogeneous bimetallic Au-Pd particles [36,37]. However, only 17% of the analyzed metal particles were actually bimetallic Au-Pd ones. Zhang et al. prepared separated Au and Pd particles on Fe(OH)_x and Fe₂O₃ supports, which resulted in better performance since they are the active sites for CO oxidation and H₂ oxidation, respectively [38]. Herzing et al. synthesized Au-Pd catalysts supported on alumina in which the fresh systems contained highly-dispersed Pd species, pure Au particles with diameters of the order of 2 nm but only a very small fraction of larger homogeneous alloy particles [39]. According to these results, the fraction of bimetallic particles observed in the catalysts prepared in this work can be considered actually very high, especially in the case of the 0.8AuPdCZ and 2.2AuPdCZ catalysts. Moreover, the size of these bimetallic particles is rather small, most of them being below 5 nm. In this sense, it seems that the synthesis procedure has been, from these points of view, successful.

3.1.4. XPS results

Table 2 lists different parameters related to the surface chemical composition of the investigated catalysts, as determined by XPS. The Zr 3d:Ce 4d ratios of the monometallic and bimetallic catalysts are around 0.43, which suggests that Zr is quite stable on the surface of the catalysts. Thus the Au:Zr and Pd:Zr molar ratios allow to following changes of the concentration of Au and Pd on the surface of the catalysts. The Au:Zr molar ratio of the monometallic Au/CZ catalyst calculated by XPS data was 0.09. In the case of the two bimetallic catalysts with lower Au:Pd ratios, the observed values for this parameter were higher than that of the monometallic Au/CZ catalyst. But the Au:Zr molar ratio of 6.4AuPdCZ catalyst with the highest Au:Pd ratio is very close to that of the monometallic Au/CZ catalyst. The XPS results indicate that the Au concentration on the surface of the bimetallic catalysts is either equal or higher than that of the monometallic Au/CZ catalyst, even though their Au loadings are slightly lower than that of Au/CZ catalyst.

Since the pretreatment applied to all the Au-containing catalysts was an oxidation, the Pd/CZ catalyst oxidized at 350 °C (Pd/CZ-O) was also measured by XPS. The Pd:Zr ratio of the Pd/CZ-O catalyst is higher than that of the Pd/CZ catalyst directly reduced at 350 °C. The Pd:Zr ratio of 0.8AuPdCZ catalyst is 0.40, which is much higher (at least 4 times) than that of Pd/CZ, in spite of its Pd loading is only 33%

higher than that of Pd/CZ. This indicates that the 0.8AuPdCZ catalyst is relatively Pd-rich on the surface compared with its actual loading. The 2.2AuPdCZ and 6.4AuPdCZ catalysts also show the same feature. In the case of 2.2AuPdCZ, the total Pd loading is roughly half that of the monometallic Pd/CZ but the Pd:Zr ratio increases in a 80%. Finally, in the bimetallic catalyst with the highest Au:Pd ratio, 6.4, the total Pd content has decreased by six times but the Pd:Zr ratio does only by a factor of 20%. Therefore, from these XPS data, we can conclude about the occurrence of a surface Pd enrichment in the bimetallic catalysts as compared to the monometallic one. The bimetallic system Au-Pd/Al₂O₃ studied by Herzing et al. also showed Pd-rich surfaces [39], in good agreement with our results.

With increasing nominal Au:Pd ratios, the Au:Pd molar ratios obtained by XPS increases, but these values are in any case much lower than those corresponding to actual Au:Pd ratios determined by ICP analysis (see Table 1). Moreover, the difference between the Au:Pd ratios obtained by XPS and ICP increases with increasing Au content. The analysis depths of Au and Pd using XPS have been calculated according to the data in literature [40,41]. For Au 4f signal, the analysis depth is between 5.4 and 5.8 nm, whereas it is only 4.6–5.0 nm in the case of Pd 3d signal. As discussed in the TEM results part, most of the metal particles are smaller than 11.6 nm for the bimetallic catalysts (if we assume that the metal particles are perfect semicircle shape), there is only a small fraction of monometallic Au particles larger than 11.6 nm in diameter. This means that Au 4f signal in the core of these Au particles might be missing in the XPS results. On the contrary, all the monometallic Pd particles found are less than 4 nm and the bimetallic Au-Pd particles are also smaller than 10 nm in diameter. This suggests that almost all Pd on the surface of the catalysts can be detected by the XPS technique. Furthermore, only a few monometallic Pd particles have been found by HAADF-STEM technique since the contrast between the support and Pd is low. XPS results reveal that the fraction of very small Pd nanoparticles must be larger than that suggested by the particle size distributions established by STEM. Unfortunately, the Au:Pd ratios obtained by XPS and XEDS cannot be compared straightforwardly since the Au:Pd ratios using XPS corresponds to ratios of the elements on the surface with maximum depth of 5.8 nm, while XEDS results are related to the total volume of the analyzed metal particles. As mentioned in the previous section, Pd contents could be underestimated due to the limitations in the contrasts of STEM-HAADF images.

The percentages of different Au and Pd species have been also estimated from quantification of experimental XPS data. Two types of Au species can be detected in all the Au containing catalysts oxidized at 250 °C as seen in Fig. 4. In all catalysts, more than 70% of Au appears at a binding energy for Au4f_{7/2} of about 84.1–84.5 eV, which corresponds either to a reduced phase of gold (most likely Au^o) or to larger Au particles [30,35]. Only a small amount of gold species (6–23%, depending on the catalyst) appear at a higher binding energy position (85.2–85.4 eV), corresponding either to more oxidized states or, alternatively, to smaller particles [35]. To simplify the discussion, the first type of gold species will be referred as

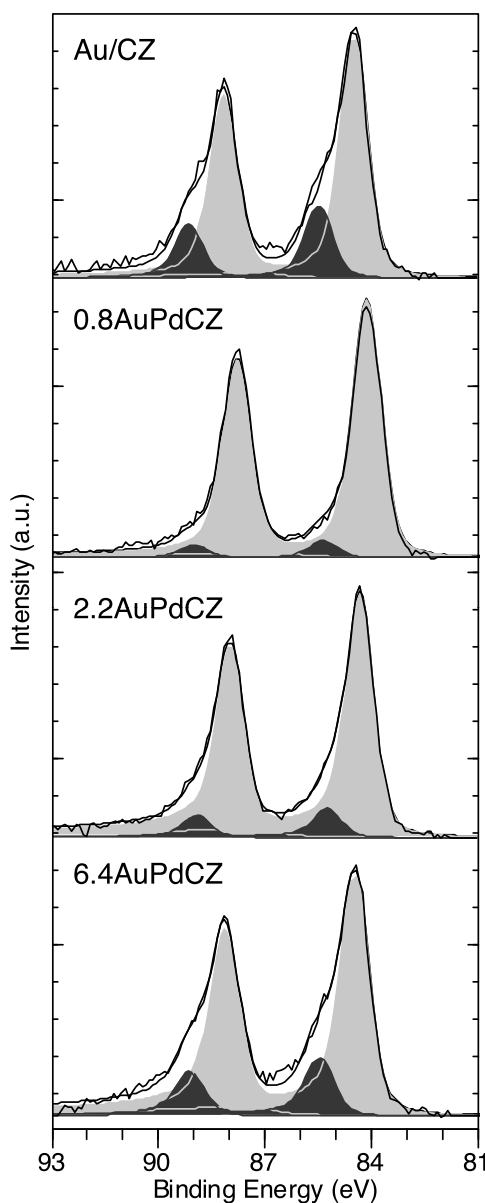


Fig. 4. Au 4f signals corresponding to the Au/CZ, 0.8AuPdCZ, 2.2AuPdCZ and 6.4AuPdCZ catalysts (from top to bottom). Light gray peaks correspond to the so-called Au[°] component, dark gray peaks to Au^{δ+}.

Au[°], while the second will be labeled as Au^{δ+}. The amount of Au^{δ+} species increases with increasing Au:Pd ratio.

Also in the case of Pd, distinct signals, which can be assigned to metallic Pd[°] and oxidized Pd^{δ+} species, are observed in all the XP spectra [22]. The percentage of oxidized Pd^{δ+} species is particularly high in the oxidized Pd/CZ-O catalyst (83%) but still amounts up to 48% in the Pd/CZ catalyst reduced at 350 °C. As it also occurs with the fraction of Au^{δ+} species, the percentage of oxidized Pd^{δ+} in the bimetallic catalysts increases with increasing Au:Pd ratio (Fig. 5 and Table 2). In any case, the fraction of oxidized species of any of the two metals is below those observed in the monometallic catalysts. Thus, the maximum fraction of oxidized Au^{δ+} amounts up to roughly 20% in the 6.4AuPdCZ catalyst whereas it represents 23% in the monometallic Au/CZ catalyst. Likewise, in the same bimetallic catalyst, a fraction of 70% Pd is present in an oxidized state, a value that it is still below the 83% detected in the monometallic catalyst submitted to the same treatment (PdCZ-O). This suggests that the simultaneous presence of the two metals contributes to

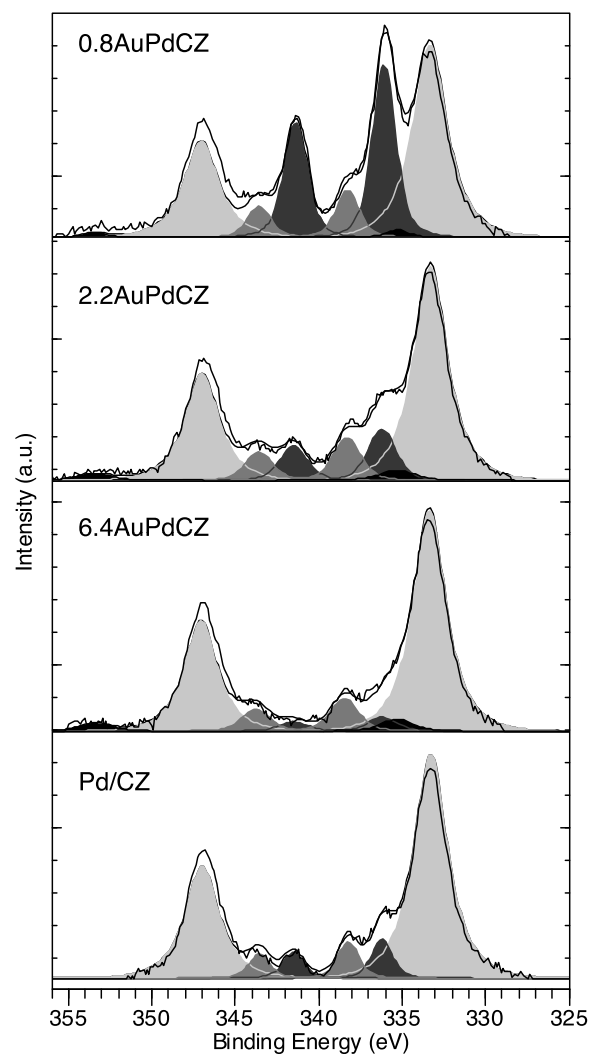


Fig. 5. Pd 3d_{5/2} signals, overlapped with Zr 3p_{3/2} and Au 4d_{5/2} corresponding to the 0.8AuPdCZ, 2.2AuPdCZ, 6.4AuPdCZ and Pd/CZ catalysts (from top to bottom). Lightest gray peaks corresponds to Zr 3p_{3/2} and Zr 3p_{1/2}, black to Au 4d_{5/2} and Au 4d_{3/2} and medium gray peaks to Pd 3d_{5/2} and Pd 3d_{3/2} (Pd[°] and Pd^{δ+}, darker and lighter gray, respectively).

an increasing fraction of them in the reduced state. In other words, with increasing Pd contents in the bimetallic catalysts, the fraction of both oxidized gold and Pd clearly decreases.

The percentage of Ce³⁺ on the surface of the different catalysts was also estimated by XPS (Table 2). Prior to their analysis in the XPS chamber, the samples were exposed to the atmosphere after their last thermal treatment and were analyzed without any further cleaning treatment in the XPS analysis chamber. Thus, the calculated Ce³⁺ percentages correspond to the residual surface Ce³⁺ species that remained reduced after exposure to atmospheric conditions. Note that the Ce³⁺ percentages on the surface of the Au/CZ and Pd/CZ-O catalysts are very similar. The fraction of Ce³⁺ increases up to 14% in the reduced Pd/CZ catalyst. For the bimetallic catalysts, the amount of Ce³⁺ decreases with increasing Au:Pd ratio. Therefore, the percentage of oxidized cerium species, Ce⁴⁺, increases in parallel with those of Pd^{δ+} and Au^{δ+}.

In summary, the XPS results indicate that increasing the total metal loading (Au + Pd) results in an increasing reduction degree of both Ce and the two metallic elements present in the bimetallic catalysts and Pd is highly-dispersed on the surface of Pd-containing catalysts.

3.1.5. Catalytic activity for the selective oxidation of glycerol

As shown in Fig. 6, the glycerol conversion increases steadily with reaction time on all the essayed catalysts until reaching total conversion. No signs of deactivation by oxygen poisoning are observed. The monometallic Pd/CZ catalyst exhibits the lowest catalytic activity for glycerol oxidation. The catalytic activity of 0.8AuPdCZ catalyst is quite similar to that of the monometallic Au/CZ catalyst. Bimetallic 2.2AuPdCZ and 6.4AuPdCZ catalysts are more active than both the monometallic Au/CZ and Pd/CZ catalysts. Therefore, a synergistic effect is observed on the Au-Pd catalysts with Au:Pd ratios of 2.2 and 6.4, especially in the case of the later.

Prati and coauthors obtained similar results and claimed that synergistic effects were present in a large range of Au:Pd molar ratios (95:5, 90:10, 80:20, 60:40 down to 20:80) on catalysts based on activated carbon as support. They reported the highest activity values in glycerol oxidation for a catalyst with a 90:10 Au:Pd molar ratio [15], a value which is very close to that of the 6.4AuPdCZ investigated here (86 mol% Au).

In the literature, turnover frequency (TOF) values were calculated based on both total amount of Au and Pd [12,13,15,18,21,22,27] and surface active sites [8–11]. The TOF_{TOTAL} and TOF_{TEM} values of the whole set of catalysts at reaction time of 3 h are compared in Table 1. The TOF_{TOTAL} values of Au/CZ and Pd/CZ catalysts are 128 and 102 h⁻¹, respectively. The TOF_{TOTAL} values of the bimetallic Au-Pd catalysts increase with increasing Au:Pd ratios. Thus, the TOF_{TOTAL} of 6.4AuPdCZ catalyst is 175 h⁻¹, which is higher than those of monometallic Au/CZ and Pd/CZ catalysts. The 2.2AuPdCZ catalyst gives a 126 h⁻¹ TOF_{TOTAL}, similar to that of the monometallic Au/CZ catalyst. Finally, the 0.8AuPdCZ catalyst is the one exhibiting the lowest TOF_{TOTAL} values among the investigated catalysts.

TOF_{TEM} values were also calculated based on the metal dispersion data obtained by STEM-HAADF. The TOF_{TEM} values of the catalysts show the same order as TOF_{TOTAL} values. The bimetallic catalysts with different Au:Pd ratios increase with decreasing Pd loadings. The 6.4AuPdCZ catalyst presents the highest TOF_{TEM} value of 515 h⁻¹ among all the catalysts.

As already mentioned, XPS results suggest that the STEM results underestimate the fraction of monometallic Pd particles in the Pd-rich catalysts due to limited visibility of the smaller Pd nanoparticles and, consequently, also the fraction of bimetallic particles in these samples. Therefore for comparison purposes it seems more reasonable to concentrate on the behavior of the Au-rich bimetallic catalyst and the monometallic ones. If we do so, it is clear that the appearance of a small fraction of bimetallic particles with more homogeneous compositions gives rises to a significant increase in the TOF_{TOTAL} values, from 128 h⁻¹ in Au/CZ to 175 h⁻¹ in 6.4AuPdCZ. According to STEM results, there are no large differences in the average particle size and metal dispersion between the different catalysts (Table 1). Therefore, these results clearly point out to a large synergistic effect between the two metals in the bimetallic catalysts.

As seen in Fig. 6, the main product of the reaction over all the catalysts is glyceric acid, as already observed on bimetallic Au-Ru catalysts [29]. The selectivity to glyceric acid is in the range from 40 to 70%, which is very valuable for final applications in fine chemistry [1,2]. The selectivity to glyceric acid shown by the Au-containing catalysts is higher than that of the Pd/CZ catalyst. The selectivity to glyceric acid slightly declines with increasing reaction time due to both further oxidation and chain cleavage processes. Thus, glycolic acid is the second main product, with selectivity values in the range 15–40%. The selectivity to glycolic acid over monometallic Pd/CZ catalyst is much higher than that of monometallic Au/CZ and bimetallic catalysts. The selectivity to tartronic acid is around 7–12% over all the catalysts at 3 h, increasing slightly with reac-

Table 3
Chemical-physical properties and quantified XPS data of the 2.2AuPdCZ catalysts oxidized at different temperatures.

Catalyst	S_{BET} (m ² g ⁻¹)	Average particle size ^a (nm)	Metal dispersion ^a (%)	Au:Pd molar ratio ^b	Ce ³⁺ in total amount of Ce (%)	Pd 3d _{5/2} (eV)		Molar ratios ^c		TOF _{TOTAL} ^d (h ⁻¹)	TOF _{TEM} ^e (h ⁻¹)				
						Au° (%)	Au ⁰⁺ (%)	Pd° (%)	Pd ⁰⁺ (%)	Zr:Ce	Au:Zr	Pd:Zr	Au:Pd		
2.2AuPdCZ	64	2.6 ± 0.1	37	8.2:1	15	84.3 (89%)	85.2 (11%)	336.2 (55%)	338.3 (45%)	0.44	0.13	0.18	0.76	126	341
2.2AuPdCZ0350	65	N.D.	N.D.	3.1 ± 0.1	19	84.2 (100%)	(0%)	336.2 (46%)	338.3 (54%)	0.41	0.11	0.15	0.71	115	N.D.
2.2AuPdCZ0450	65	36	2.9:1	20	20	84.2 (100%)	(0%)	336.2 (45%)	338.3 (55%)	0.41	0.10	0.14	0.73	113	314
2.2AuPdCZ0700	60	7.3 ± 0.3	16	1.7:1	35	83.9 (100%)	(0%)	336.2 (47%)	338.4 (53%)	0.40	0.05	0.07	0.73	141	881

N.D.: Not determined.

^a Average particle size and metal dispersion were determined by STEM technique.

^b Au:Pd molar ratio was obtained by STEM-XEDS technique.

^c Molar ratios were calculated by XPS data.

^d TOF_{TOTAL} values were calculated based on total amount of metals of the catalysts when the reaction time is 3 h.

^e TOF_{TEM} values were calculated based on the metal dispersion obtained by STEM-HAADF when the reaction time is 3 h.

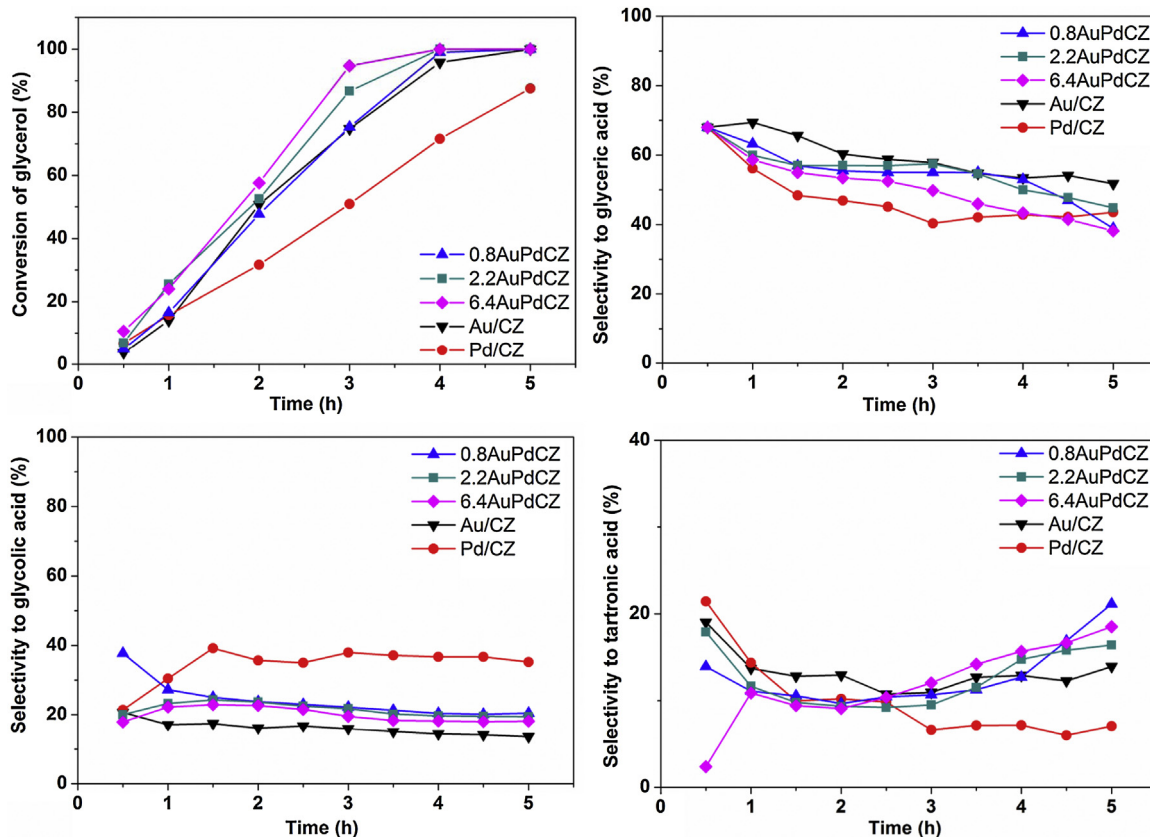


Fig. 6. Catalytic activity for glycerol oxidation over the catalysts. Reaction conditions: 60 °C, P_{O₂} = 3 bar, catalyst amount: 700 mg, NaOH:glycerol = 2 mol:mol, 150 mL of 0.3 M glycerol solution.

tion time over Au-containing catalysts, but remaining constant for monometallic Pd/CZ catalyst. As mentioned before, the reaction pathway of glycerol oxidation is very complicated and depends on the reaction conditions, active site of catalyst and metal particle size [1–3]. However, it is widely accepted that glycerol oxidation can follow two routes: one leading to C–C scission to produce glycolic acid, the other to glyceric acid and tartronic acid [21]. The observed selectivity values indicate that on the Au-containing catalysts, both Au/CZ and bimetallic ones, the dominant reaction route is that leading to increasing oxidation of glycerol whereas in the case of Pd/CZ C–C bond scission competes better with oxidation. It is also important to stress, that the total selectivity to glyceric, glycolic and tartronic acids over all the catalysts is above 80%, showing therefore all of them a high potential in the conversion of glycerol to products with commercial interest. Formic acid can be detected over all the catalysts, but always with very low selectivity (only 1%). The selectivity to oxalic acid in all the cases is very low and slightly increases with reaction time over Au-containing catalysts. No other compounds are detected suggesting the formation of some CO₂.

3.2. Effect of the oxidation temperature on the performance of the 2.2AuPdCZ catalyst

Since the bimetallic Au-Pd catalysts demonstrate the occurrence of synergistic effects, it is desirable to study the influence on the catalytic performance of the temperature used during their activation under oxidizing conditions. The 2.2AuPdCZ catalyst was the one selected to investigate the effect of the oxidation temperature.

3.2.1. Textural and structural properties

Table 3 shows the BET specific surface areas of 2.2AuPdCZ catalyst oxidized at different temperatures. Note that oxidation at 350

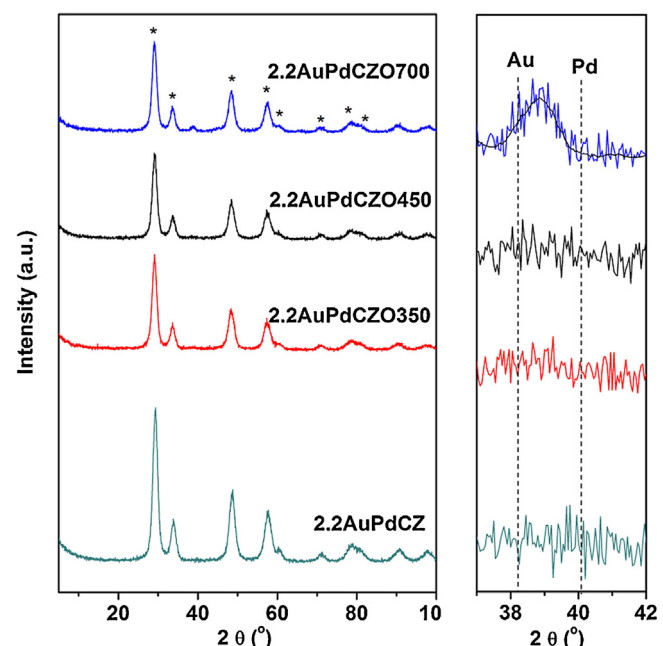


Fig. 7. XRD patterns of bimetallic 2.2AuPdCZ catalyst oxidized at different temperatures. *Diffraction peaks of fluorite structure for Ce_{0.62}Zr_{0.38}O₂ mixed oxide.

and 450 °C does not lead to any significant change of the surface area of the catalyst. Only a slight decline of the surface area takes place after oxidation at the highest temperature (700 °C), which evidences a high textural stability of the catalyst.

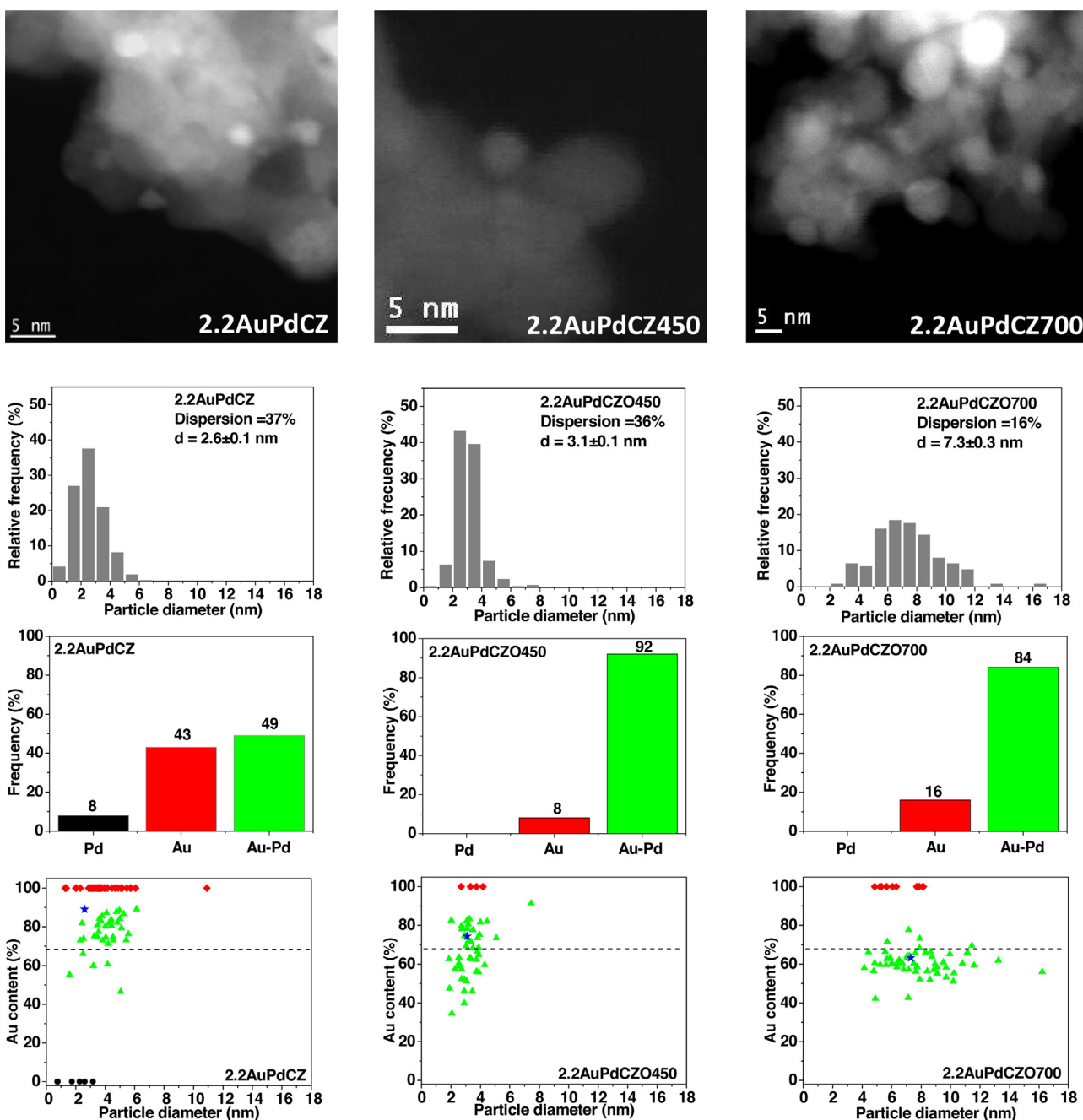


Fig. 8. STEM-HAADF images, particle size distribution, frequency of Au, Pd and Au-Pd metal particles, and relationship between particle size and Au content of the 2.2AuPdCZ, 2.2AuPdCZO450 and 2.2AuPdCZO700 catalysts. The dash line is the Au content according to ICP analysis for each catalyst. Solid black circles correspond to monometallic Pd particles; solid red diamonds correspond to monometallic Au particles; solid green up-triangles correspond to bimetallic Au-Pd particles. Solid blue star corresponds to the average particle size and the average Au content calculated by XEDS data. (For interpretation of the references to colour in this figure legend, the reader is referred to the web version of this article.)

XRD results also confirm that the fluorite type structure of ceria-zirconia maintains for all the bimetallic catalysts oxidized at increasing temperatures. However, a small and wide diffraction peak at 38.8° can be observed in the 2.2AuPdCZO700 catalyst (Fig. 7). The appearance of this peak between Au {111} (38.2°) and Pd {111} (40.1°) suggests both the formation of a Au-Pd alloy and an increase of the metal particle size after oxidation at 700°C [42,43].

3.2.2. STEM results

Fig. 8 shows representative STEM-HAADF images and particle size distribution of 2.2AuPdCZ oxidized at 250, 450 and 700 °C. The

metal particle size is still in the range from 1 to 5 nm after oxidation at 450°C . The average metal particle size increases slightly from 2.6 to 3.1 nm, while still maintaining a high dispersion, 36%. Oxidation at 700°C causes a larger increase of the average particle size to 7.3 nm and a substantial decline in the metal dispersion (16%). Metal particle diameters fall now within a much wider range, from 3 to 16 nm. These results are in good agreement with XRD.

Fig. 8 also includes information about the frequency of the different types of metal nanoparticles, present in the 2.2AuPdCZ catalyst, as a function of the oxidation temperature. Quite remarkably, the increase in oxidation temperature up to 450°C leads to a large

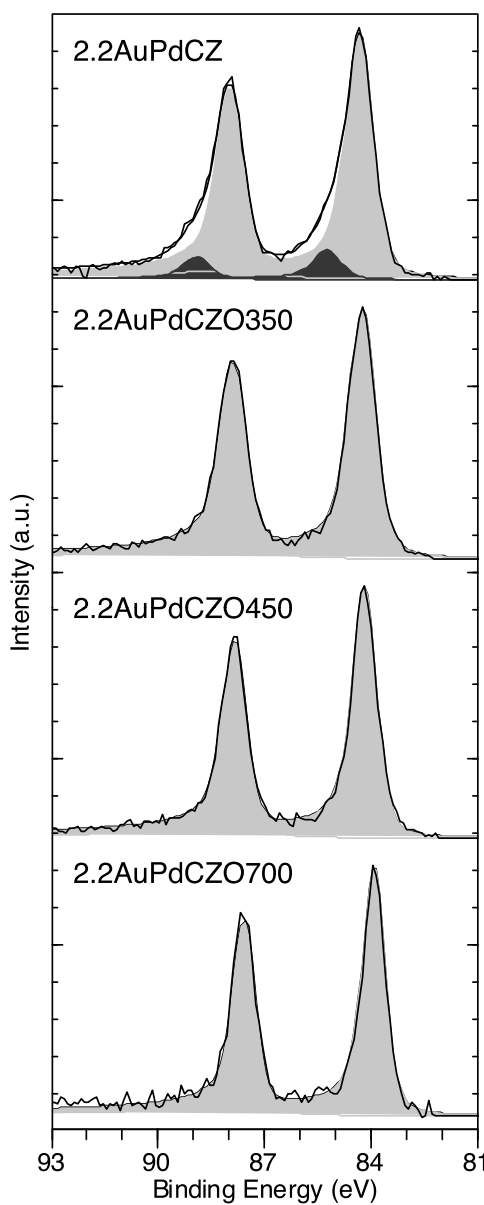


Fig. 9. Au 4f signals corresponding to 2.2AuPdCZ catalysts oxidized at different temperatures (from top to bottom): 250, 350, 450 and 700 °C. Light gray peaks correspond to the so-called Au° component, dark gray peaks to Au δ^+ .

increase in the frequency of bimetallic Au-Pd particles, from 49% to 92%. No Pd nanoparticles are found in this catalyst and the frequency of monometallic Au decreases down to 8%. As it occurs in the 2.2AuPdCZ catalyst, the size of most of the particles, either mono or bimetallic, are in the 2–5 nm size range.

Another important question refers to the effect of increasing the oxidation temperature on the composition of the bimetallic particles. Oxidation at 450 °C leads to bimetallic nanoparticles whose composition varies in the same range as in the catalyst oxidized at 250 °C, i.e. from 35 to 90 mol% Au. This indicates that oxidation at 450 °C affects only very slightly the particle size, drastically increases the fraction of bimetallic Au-Pd nanoparticles but the composition of these nanoparticles is similar to those existing in the catalyst oxidized at 250 °C.

After oxidation at 700 °C, no monometallic Pd nanoparticles are detected and the frequency of bimetallic Au-Pd nanoparticles (84%) remains quite high and quite close to that observed after oxidation at 450 °C. The composition-size diagrams provide

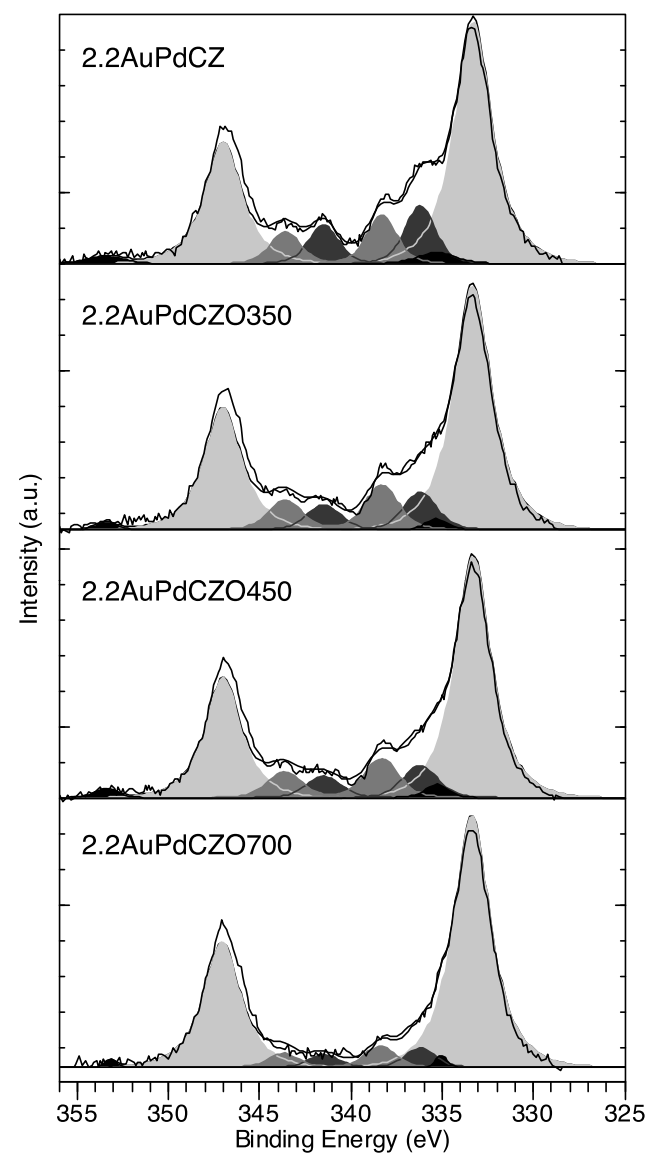


Fig. 10. Pd 3d $_{5/2}$ signals, overlapped with Zr 3p $_{3/2}$ and Au 4d $_{5/2}$ corresponding to 2.2AuPdCZ catalysts oxidized at different temperatures (from top to bottom): 250, 350, 450 and 700 °C. Lightest gray peaks corresponds to Zr 3p $_{3/2}$ and Au 3p $_{1/2}$, black to Au 4d $_{5/2}$ and Au 4d $_{3/2}$, and medium gray peaks to Pd 3d $_{5/2}$ and Pd 3d $_{3/2}$ (Pd° and Pd δ^+ , darker and lighter gray, respectively).

two more interesting details: firstly, it reveals that the increase of particle size affects especially the bimetallic nanoparticles; secondly, very important, increasing the oxidation temperature up to 700 °C shrinks very clearly the composition range of the bimetallic particles, which now lies in a narrower range around the actual Au loading, 68 mol%. Table 3 also lists the Au:Pd molar ratios of bimetallic catalysts oxidized at different temperatures calculated by XEDS data. The Au:Pd molar ratio of 2.2AuPdCZ catalyst oxidized at 250 °C is much higher than the one obtained by ICP results. However, the Au:Pd ratios of 2.2AuPdCZ catalyst after oxidation at 450 and 700 °C are very close to ICP results. This result also confirms that homogeneous bimetallic particles form after oxidation at 450 and 700 °C.

Summarizing these STEM results, oxidation at 450 and 700 °C leads to some sintering of metal particles (especially in the case of 700 °C) and to the formation of a higher fraction of bimetallic Au-Pd nanoparticles with more homogeneous composition.

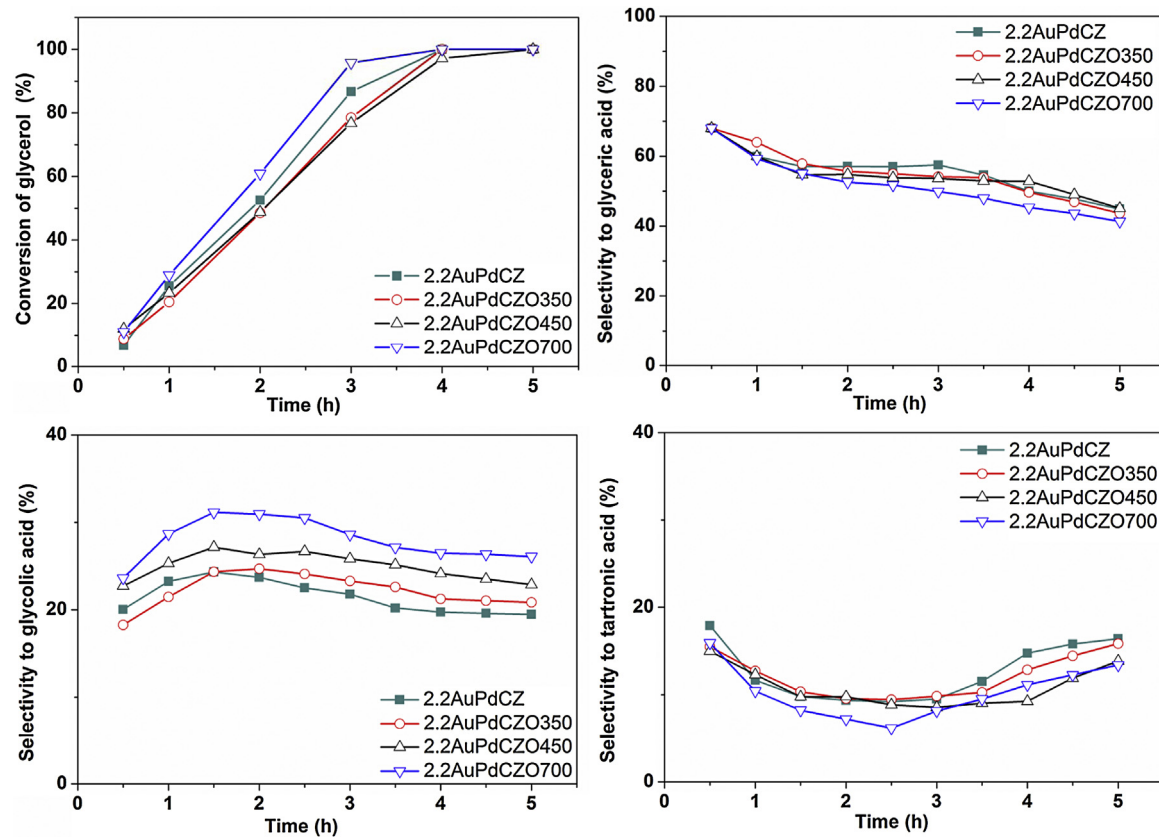


Fig. 11. Catalytic activity for glycerol oxidation over bimetallic 2.2AuPdCZ catalyst oxidized at different temperatures. Reaction conditions: 60 °C, P_{O₂} = 3 bar, catalyst amount: 700 mg, NaOH:glycerol = 2 mol:mol, 150 mL of 0.3 M glycerol solution.

3.2.3. XPS results

Table 3 contains the XPS results corresponding to the 2.2AuPdCZ catalyst oxidized at increasing temperatures. The Au:Zr and Pd:Zr molar ratios decrease slightly with increasing oxidation temperature up to 450 °C and then much more steeply at 700 °C, clearly suggesting that the occurrence of Au and Pd agglomeration at the highest oxidation temperature. However, the Au:Pd molar ratio remains almost constant at different oxidation temperatures, suggesting an homogenous distribution of both elements after the sintering process. The 2.2AuPdCZ catalysts oxidized at 350, 450 and 700 °C still show Pd-rich surface as the bimetallic catalyst oxidized at 250 °C.

As shown in section 3.1.4, both Au° (89%) and Au^{δ+} (11%) are found on the 2.2AuPdCZ catalyst. After oxidation at 350, 450 and 700 °C, positive Au^{δ+} species disappear and the only visible XPS signal corresponds to Au° (Fig. 9). Concerning the XPS signal of Pd, oxidation at 350, 450 or 700 °C leads to oxidation of Pd in a slightly larger extent, as compared to that observed at 250 °C (Fig. 10). The percentage of Pd^{δ+} increases from 45 to 55% and the percentage of Pd° decreases accordingly (Table 3). This result indicates that the oxidation states of Au and Pd do not change after oxidation at temperatures higher than 350 °C. Zhang et al. obtained similar results over Au-Pd/Fe(OH)_x catalyst [38]. In samples calcined at low temperatures, they reported the presence of Au and Pd in both reduced and partially oxidized states. After calcination at 500 °C, Au oxidized species disappear completely and only metallic Au species are found, but Pd species still maintain both oxidized and metallic oxidation states [38].

Concerning the influence of increasing the oxidation temperature on the oxidation state of the support, we should take into

account that treatments at high temperatures in noble metal loaded systems can reduce Ce⁴⁺ to Ce³⁺, even under an oxidizing environment [44]. Note in fact that the percentage of Ce³⁺ increases from 15 to 35% when the oxidation temperature increases from 250 to 700 °C. The Zr:Ce molar ratios decrease slightly from 0.44 to 0.40 with increasing oxidation temperatures.

3.2.4. Catalytic activity for the selective oxidation of glycerol

The values of the glycerol conversion over the 2.2AuPdCZ catalyst oxidized at increasing temperatures are shown in Fig. 11. The catalytic activities of 2.2AuPdCZO350 and 2.2AuPdCZO450 are quite similar and slightly lower than that of the 2.2AuPdCZ catalyst. However, the 2.2AuPdCZ catalyst oxidized at 700 °C exhibits the highest catalytic activity among the bimetallic catalysts oxidized at different temperatures. As deduced from XRD, STEM and XPS results, the metal particle size increases after oxidation at 700 °C but the bimetallic Au-Pd particles, which consist of the major fraction after oxidation at temperatures above 350 °C, become much more homogeneous in composition, around its actual molar ratio of 68:32. Therefore, it seems clear that the formation of homogeneous bimetallic Au-Pd particles promotes the catalytic activity for glycerol oxidation.

Previous works studying the performance of Au supported on activated carbon and carbon nanotubes have reported that the surface chemistry of the support plays an important role in glycerol oxidation [8,11,24]. Surface oxygenated acid groups on carbon supports seem especially deleterious for catalytic activity [8,11]. For the Au-Pd/Ce_{0.62}Zr_{0.38}O₂ catalysts studied here, there is no direct correlation between the reduction degree of Ce and their catalytic activities. The Au-Pd/Ce_{0.62}Zr_{0.38}O₂ catalyst with higher

Au:Pd ratios and lower reduction degree of Ce exhibits higher catalytic activity. In the series of catalysts obtained by increasing the oxidation temperature, oxidation at 700 °C leads to a higher reduction degree of Ce, which is in this case accompanied by an increase of catalytic activity. This could be attributed to the fact that the percentage of Ce³⁺ determined by XPS reflect the state of the surface after the synthesis procedure, which might differ from that under actual reaction conditions (aqueous solution, at 60 °C, under 3 bar in an autoclave). Nevertheless this is not the only structural factor which is modified, since the homogeneity of the bimetallic catalysts increases with oxidation temperature. It is not possible to separate both contributions to the enhanced catalytic activity observed with the increase of oxidation temperature. Further studies considering catalysts in which each parameter is separately modified are necessary to have a proper insight into the influence of the redox state of the support. In principle, such studies would also need take into account the state of the support under conditions close to those employed during the catalytic essays, i.e. in the presence of oxygen at a 3 bar pressure and 60 °C. Such an approach is outside the scope of the present work, which is aimed at elucidating more general questions.

Table 3 shows the TOF_{TOTAL} and TOF_{TEM} values at reaction time of 3 h. Since 2.2AuPdCZ catalysts oxidized at different temperatures consist of the same amount of Au and Pd, the TOF_{TOTAL} values present the same trend as glycerol conversion. However, the TOF_{TEM} value of 2.2AuPdCZ700 increases drastically from 341 to 881 h⁻¹, almost threefold of 2.2AuPdCZ catalyst because the metal dispersion of this catalyst decreases to 16%. As it has been discussed above, synergistic effect of 2.2AuPdCZ700 might be due to the formation of homogeneous Au-Pd bimetallic particles.

As seen in **Fig. 11**, the selectivities to glyceric and tartronic acids are similar over the bimetallic catalysts oxidized at different temperatures. In contrast, the selectivity to glycolic acid increases with increasing oxidation temperature. This might be due to the change in size and/or composition of the metal nanoparticles with oxidation temperature. The selectivity values towards formic acid and oxalic acid are less than 5% for all the catalysts, which is in fact very low. It is important to stress at this point that selectivity trends in glycerol oxidation still remain as an open question in which the separate contribution of different factors such as size, composition or morphology of the metal particles or the role of the support and reaction conditions has not been clarified yet [11].

4. Conclusions

Bimetallic Au-Pd catalysts supported on ceria-zirconia mixed oxide catalysts with different Au:Pd molar ratios (0.8, 2.2 and 6.4) maintaining Au loadings constant have been synthesized using a simultaneous deposition-precipitation method. Remarkably, this synthesis approach has allowed us preparing catalysts containing metal nanoparticles with diameters mostly in the 1–5 nm range. This method leads to systems of bimetallic nanoparticles whose individual compositions vary in a wide range spanning from monometallic (Au, Pd) to bimetallic Au-Pd ones with largely different Au:Pd ratios. A synergistic effect between Au and Pd has been observed on these catalysts in the selective oxidation of glycerol. Catalysts with higher Au:Pd molar ratios show better catalytic activities in this reaction. A valuable observation is that increasing the temperature of the oxidation pretreatment used to activate the catalyst results in a clear compositional homogenization, which brings the Au:Pd molar ratios of most of the particles present in the catalyst to values quite close to that corresponding to the actual one obtained by ICP. Also important, the catalytic activity for selective oxidation of glycerol is improved after oxidation at 700 °C. Such

improvement can be clearly attributed to the formation of more compositionally homogenous bimetallic alloy particles.

Taking the last observation into account in parallel with the fact that during the oxidation at high temperature the metal particles grow significantly in size, it seems clear that the synthesis of catalysts containing a system of small (<5 nm), compositionally homogeneous particles, with compositions in the 70:30–90:10 Au:Pd range, could lead to further improvements in the catalytic performance of Au-Pd catalysts in the glycerol oxidation reaction.

Acknowledgements

This work has been supported by the Ministry of Science and Innovation of Spain/FEDER Program of the EU (Project: MAT 2013-40823-R, CSD2009-00013), ESTEEM2 (FP7-INFRASTRUCTURE-2012-1-312483, Junta de Andalucía (FQM334 and FQM110 and Project: FQM3994) and PEst-C/EQB/LA0020/2013, financed by FEDER through COMPETE-Programa Operacional Factores de Competitividade (Portugal). It is also partially supported by Acção Integrada Luso-Espanhola N° E28/11 (Portugal) and Acciones Integradas with reference number AIB2010PT-00377 (Spain). J. J. Delgado, A. B. Hungria and X. Chen thank the program of "Ramón y Cajal" from Ministry of Science and Innovation of Spain.

References

- [1] B. Katryniok, H. Kimura, E. Skrzynska, J.-S. Girardon, P. Fongarland, M. Capron, R. Ducoulombier, N. Mimura, S. Paul, F. Dumeignil, *Green Chem.* 13 (2011) 1960–1979.
- [2] M. Pagliaro, R. Ciriminna, H. Kimura, M. Rossi, C.D. Pina, *Angew. Chem. Int. Ed.* 46 (2007) 4434–4440.
- [3] M. Besson, P. Gallezot, *Catal. Today* 57 (2000) 127–141.
- [4] H. Kimura, K. Tsuto, T. Wakisaka, Y. Kazumi, Y. Inaya, *Appl. Catal. A-Gen.* 96 (1993) 217–228.
- [5] R. Garcia, M. Besson, P. Gallezot, *Appl. Catal. A-Gen.* 127 (1995) 165–176.
- [6] S. Carretti, P. McMorn, P. Johnston, K. Griffin, G.J. Hutchings, *Chem. Commun.* (2002) 696–697.
- [7] S. Carretti, P. McMorn, P. Johnston, K. Griffin, C.J. Kiely, G.J. Hutchings, *Phys. Chem. Chem. Phys.* 5 (2003) 1329–1336.
- [8] E.G. Rodrigues, M.F.R. Pereira, X. Chen, J.J. Delgado, J.J.M. Órfão, *J. Catal.* 281 (2011) 119–127.
- [9] E.G. Rodrigues, M.F.R. Pereira, J.J. Delgado, X. Chen, J.J.M. Órfão, *Catal. Commun.* 16 (2011) 64–69.
- [10] E.G. Rodrigues, S.A.C. Carabineiro, J.J. Delgado, X. Chen, M.F.R. Pereira, J.J.M. Órfão, *J. Catal.* 285 (2012) 83–91.
- [11] E.G. Rodrigues, J.J. Delgado, X. Chen, M.F.R. Pereira, J.J.M. Órfão, *Ind. Eng. Chem. Res.* 51 (2012) 15884–15894.
- [12] C.L. Bianchi, P. Canton, N. Dimitratos, F. Porta, L. Prati, *Catal. Today* 102–103 (2005) 203–212.
- [13] N. Dimitratos, F. Porta, L. Prati, *Appl. Catal. A-Gen.* 291 (2005) 210–214.
- [14] E.G. Rodrigues, S.A.C. Carabineiro, X. Chen, J.J. Delgado, J.L. Figueiredo, M.F.R. Pereira, J.J.M. Órfão, *Catal. Lett.* 141 (2011) 420–431.
- [15] A. Villa, C. Campione, L. Prati, *Catal. Lett.* 115 (2007) 133–136.
- [16] W.C. Ketchie, M. Murayama, R.J. Davis, *J. Catal.* 250 (2007) 264–273.
- [17] L. Prati, M. Rossi, *J. Catal.* 176 (1998) 552–560.
- [18] D. Wang, A. Villa, F. Porta, D.S. Su, L. Prati, *Chem. Commun.* (2006) 1956–1958.
- [19] D. Wang, A. Villa, F. Porta, L. Prati, D.S. Su, *J. Phys. Chem. C* 112 (2008) 8617–8622.
- [20] L. Prati, A. Villa, F. Porta, D. Wang, D.S. Su, *Catal. Today* 122 (2007) 386–390.
- [21] N. Dimitratos, J.A. Lopez-Sánchez, D. Lennon, F. Porta, L. Prati, A. Villa, *Catal. Lett.* 108 (2006) 147–153.
- [22] N. Dimitratos, J.A. Lopez-Sánchez, J.M. Anthonykutty, G. Brett, A.F. Carley, R.C. Tiruvalam, A.A. Herzing, C.J. Kiely, D.W. Knight, G.J. Hutchings, *Phys. Chem. Chem. Phys.* 11 (2009) 4952–4961.
- [23] S.-S. Liu, K.-Q. Sun, B.-Q. Xu, *ACS Catal.* 4 (2014) 2226–2230.
- [24] C. Xu, Y. Du, C. Li, J. Yang, G. Yang, *Appl. Catal. B-Environ.* 164 (2015) 334–343.
- [25] P. Lakshmanan, P.P. Upare, N.-T. Le, Y.K. Hwang, D.W. Hwang, U.-H. Lee, H.R. Kim, J.-S. Chang, *Appl. Catal. A-Gen.* 468 (2013) 260–268.
- [26] S. Demirel, P. Kern, M. Lucas, P. Claus, *Catal. Today* 122 (2007) 292–300.
- [27] L. Wang, W. Zhang, S. Zeng, D.S. Su, X. Meng, F. Xiao, *Chin. J. Chem.* 30 (2012) 2189–2197.
- [28] J. Kašpar, P. Fornasiero, M. Graziani, *Catal. Today* 50 (1999) 285.
- [29] L.E. Chinchilla, C.M. Olmos, A. Villa, A. Carlsson, L. Prati, X. Chen, G. Blanco, J.J. Calvino, A.B. Hungria, *Catal. Today* 253 (2015) 178–189.
- [30] J.M. Cies, E. del Rio, M. Lopez-Haro, J.J. Delgado, G. Blanco, S. Collins, J.J. Calvino, S. Bernal, *Angew. Chem. Int. Ed.* 49 (2010) 9744–9748.
- [31] J.M. Cies, J.J. Delgado, M. Lopez-Haro, R. Pilasombat, J.A. Pérez-Omil, S. Trasobares, S. Bernal, J.J. Calvino, *Chem. Eur. J.* 16 (2010) 9536–9543.

- [32] E. del Río, G. Blanco, S. Collins, M. López-Haro, X. Chen, J.J. Delgado, J.J. Calvino, S. Bernal, *Top. Catal.* 54 (2011) 931–940.
- [33] E. del Río, S.E. Collins, A. Aguirre, X. Chen, J.J. Delgado, J.J. Calvino, S. Bernal, *J. Catal.* 316 (2014) 210–218.
- [34] M. López-Haro, J.J. Delgado, J.M. Cies, E. del Rio, S. Bernal, R. Burch, M.A. Cauqui, S. Trasobares, J.A. Pérez-Omil, P. Bayle-Guillemaud, J.J. Calvino, *Angew. Chem. Int. Ed.* 49 (2010) 1981–1985.
- [35] C.M. Olmos, L.E. Chinchilla, J.J. Delgado, A.B. Hungría, G. Blanco, J.J. Calvino, X. Chen, *Catal. Lett.* 146 (2016) 144–156.
- [36] J. Xu, T. White, P. Li, C. He, J. Yu, W. Yuan, Y.-F. Han, *J. Am. Chem. Soc.* 132 (2010) 10398–10406.
- [37] A. Maeland, T.B. Flanagan, *Can. J. Phys.* 42 (1964) 2364–2366.
- [38] B. Qiao, A. Wang, M. Takahashi, Y. Zhang, J. Wang, Y. Deng, T. Zhang, *J. Catal.* 279 (2011) 361–365.
- [39] A.A. Herzing, A.F. Carley, J.K. Edwards, G.J. Hutchings, C.J. Kiely, *Chem. Mater.* 20 (2008) 1492–1501.
- [40] C. Powell, A. Jablonski, NIST electron inelastic-mean-free-path database, version 1.2, in: SRD 71, National Institute of Standards and Technology, Gaithersburg, MD, 2010.
- [41] W.H. Gries, *Surf. Interface Anal.* 24 (1996) 38–50.
- [42] A.M. Venezia, L.F. Liotta, G. Pantaleo, V. La Parola, G. Deganello, A. Beck, Zs. Koppány, K. Frey, D. Horváth, L. Guczi, *Appl. Catal. A: Gen.* 251 (2003) 359–368.
- [43] X. Wei, X.-F. Yang, A.-Q. Wang, L. Li, X.-Y. Liu, T. Zhang, C.-Y. Mou, J. Li, *J. Phys. Chem. C* 116 (2012) 6222–6232.
- [44] J. Fan, X. Wu, R. Ran, D. Weng, *Appl. Surf. Sci.* 245 (2005) 162–171.